Acta Crystallographica Section B
Structural Science
ISSN 0108-7681

Original disorder–order transition related to electronic and magnetic properties in the thermoelectric misfit phase $[Ca_2CoO_3][CoO_2]_{1.62}$

Hervé Muguerra* and Dominique Grebille

CRISMAT-ENSICAEN Laboratory, UMR CNRS 6508, 6 Bd Maréchal Juin, F-14050 Caen CEDEX, France

Correspondence e-mail: herve.muguerra@ensicaen.fr

Received 4 July 2008
Accepted 18 September 2008

A structural phase transition is shown around 400 K for the thermoelectric lamellar misfit cobalt oxide $[Ca_2CoO_3]$-$[CoO_2]_{1.62}$. This transition is related to a rearrangement of the central [CoO] layer of the $[Ca_2CoO_3]$ slab of this structure, characterized by a commensurate intrinsic modulation $\mathbf{q}_2 = \frac{2}{3}\mathbf{a}^* - \frac{1}{3}\mathbf{c}^*$. The partial residual disorder related to split Co and O atomic sites along the misfit *b* direction disappears and one can describe this layer with its triple chains as a modulated configuration with a regular and not distorted periodicity along **b**. This phase transition is associated with small changes observed in the transport and magnetic properties as a function of temperature.

1. Introduction

Thermoelectric generation systems can directly convert heat energy into electrical energy or *vice versa*, which provides an effective route to use the waste heat from automobiles, factories and so on, or conversely to cool down electronic devices for example. These systems should possess high conversion efficiency and should also be composed of non-toxic and abundantly available elemental materials having high chemical stability in air, even at temperatures of 800−1000 K. Recently, the layered cobalt-based oxide materials have been widely studied in light of their promising thermoelectric properties. Among various cobalt-based oxide materials, $Ca_3Co_4O_9$ (CCO) has the dimensionless figure of thermoelectric merit $ZT = S^2T/\rho\kappa$ (S is the Seebeck coefficient, T is the absolute temperature, ρ is the electrical resistivity and κ is the thermal conductivity) about 1 near 1000 K, which suggests that CCO can be considered as a very important candidate for thermoelectric applications (Li *et al.*, 1999; Funahashi *et al.*, 2000; Miyazaki *et al.*, 2000).

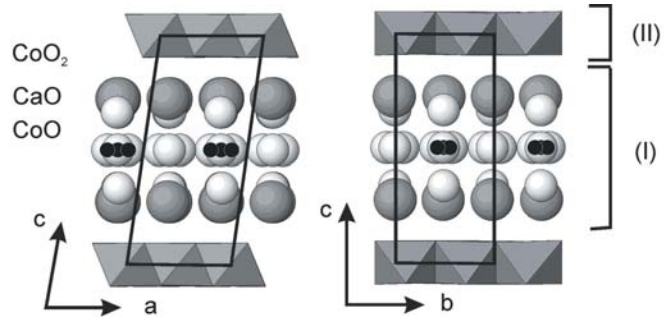

Figure 1
Schematic representation of the average structure of CCO. Both subsystems can be easily recognized (only the crystal cell of subsystem 1 is drawn). The central [CoO] layer of subsystem 1 is characterized by split Co and O atom sites.

Table 1
Crystal data and structure refinement results of CCO at 473 K.

		$[Ca_2CoO_3][CoO_2]_{1.62}$
Chemical formula		$Ca_2Co_{2.511}O_{6.138}$
Formula weight (g mol^{-1})		326.32
Crystal size (mm)		0.08 × 0.13 × 0.025
Crystal system		Monoclinic
Cell parameters (Å, °)		$a_1 = a_2 = 4.839$ (1)
		$b_1 = \delta b_2 = 4.553$ (1)
		$c_1 = c_2 = 10.858$ (3)
		$\beta = 98.12$ (2)
$\delta = b_1/b_2$		1.6157 (7)
Superspace group		$C2/m(1\delta0)(\alpha0\gamma)gm$
Modulation wavevector		$\mathbf{q}_1 = \frac{13}{8}\mathbf{b}_2^*$
		$\mathbf{q}_2 = \frac{2}{3}\mathbf{a}_1^* - \frac{1}{3}\mathbf{c}_1^*$
Z		2
ρ (g cm^{-3})/μ (mm^{-1})		4.5746/10.849
Wavelength (Å)		0.70926
Temperature (K)		473
Internal consistency factor R_{int} (%; after absorption correction)		
First subsystem		2.72/2.85
Second subsystem		2.85/2.85
Modulation $\mathbf{q}_1$		3.85/3.85
Modulation $\mathbf{q}_2$		3.82/4.70
T_{min}/T_{max}		
First subsystem		0.39/0.85
Second subsystem		0.42/0.85
Modulation $\mathbf{q}_1$		0.37/0.85
Modulation $\mathbf{q}_2$		0.39/0.86
Number of paramaters actually refined		67
Weighting scheme		$1/\sigma^2$
Number of unique reflections [with $I \geq 3\sigma(I)$]		Corresponding reliability factor, R/wR
Total	2014	0.0337/0.0234
Main reflections	582	0.0264/0.0208
First subsystem	328	0.0344/0.0221
Second subsystem	184	0.0236/0.0215
Common reflections	70	0.0169/0.0170
Modulation $\mathbf{q}_1$	627	0.1384/0.1128
Modulation $\mathbf{q}_2$	804	0.0594/0.0483
Residues (e Å^{-3})		−1.34, 1.39

CCO is composed of two subsystems stacked along the *c* direction: a rock-salt (RS) block sandwiching $[CoO_2]$ layers (Fig. 1). This phase should be preferentially written as $[Ca_2CoO_3][CoO_2]_{1.62}$, where $[Ca_2CoO_3]$ describes the RS block, $[CoO_2]$ the second subsystem and $b_1/b_2 = 1.62$ the aperiodic ratio. The $[CoO_2]$ layers are formed by a pseudo-hexagonal network of edge-sharing CoO_6 octahedra and *RS* blocks by a succession of three layers along the stacking *c* direction (CaO–CoO–CaO). Several structural studies have been published about this compound (Miyazaki *et al.*, 2002; Ling *et al.*, 2007). Powder X-ray diffraction experiments have proved the existence of a splitting of the atoms of the central layer [CoO] (Lambert *et al.*, 2001). Recently a partial ordering within the [CoO] layer has been proposed from a single-crystal X-ray diffraction study (Muguerra *et al.*, 2008). The observation of new satellite reflections, characterizing a new intrinsic modulation in the RS block ($\mathbf{q}_2 = \frac{2}{3}\mathbf{a}^* - \frac{1}{3}\mathbf{c}^*$), and a structure refinement using the five-dimensional superspace formalism (Yamamoto, 1992) prove that the [CoO] layer can be described with triple chains aligned along the misfit **b** direction. The reader should first refer to this first structural description which is the basic model for the present work.

For a better understanding of the CCO thermoelectric properties, which are still in debate, different comparisons with related materials like sodium cobaltate Na_xCoO_2 (Terasaki *et al.*, 1997) or other misfit cobalt oxides have been developed. Thermoelectricity clearly finds its origin in the $[CoO_2]$ sheets present in all of these structures. An accurate examination of this layer proves that it always presents exactly the same distortion of the CoO_6 octahedra (Muguerra *et al.*, 2008; Grebille *et al.*, 2007). This outlines the fact that the achievement of good thermoelectric performance needs a particular organization of the O—Co—O angles and the Co—O distances. So, conversely, the measured differences of physical properties are to be related to the rest of the structure, *i.e.* the RS block or the intermediate deficient cationic layer. As a matter of fact, one can easily imagine different doping features or coulombic interactions which can act differently on the entropy of localized spins or to electronic correlations (Koshibae *et al.*, 2000; Xiang & Singh, 2007; Bobroff *et al.*, 2007; Limelette *et al.*, 2005, 2006). In particular, the strong bonding resulting from the short Ca—O bonds between the two subsystems is globally averaged along the misfit direction. Indeed the atomic environments are never reproduced in the same manner, the modulated displacements of the Ca and O atoms are such that a practically constant Ca—O distance of 2.3 Å is observed between the two subsystems. The question is how a structural modification of the RS block can influence physical properties inherent to the $[CoO_2]$ layers. For this purpose, an accurate structural description of the corresponding layers is also very important.

CCO presents successive magnetic transitions, at low temperatures and 400–600 K (Sugiyama, Brewer *et al.*, 2003; Sugiyama, Xia & Tani, 2003), and some small magnetic susceptibility and electrical resistivity anomalies around 400 K (Masset *et al.*, 2000). A single-crystal X-ray diffraction study at different temperatures is interesting in order to correlate these magnetic and electrical features to structural transitions, in particular within the RS block.

2. Experimental

Single crystals were grown by the flux method (Xia *et al.*, 2005). $CaCO_3$ and Co_3O_4 were mixed with a cationic composition of Ca:Co = 2:2.62. The resulting powder was mixed with a $SrCl_2$ flux (weight ratio of 1:2) and heated in a Pt crucible at 1173 K for 12 h, then cooled down to 623 K at a rate of 5 K h^{-1} before being furnace-cooled. The plate-like single crystals have a typical hexagonal morphology with an area of 0.02 mm^2 and a thickness of 30 µm.

Single-crystal X-ray diffraction studies were performed at different temperatures using Mo $K\alpha$ radiation with a Nonius KappaCCD diffractometer. A high-temperature Cyberstar attachment was used for these studies (Argoud & Capponi, 1984). The high temperature was obtained by blowing a stream of hot air on the crystal. The temperature was regulated within ± 3 K. Different basic data collections were

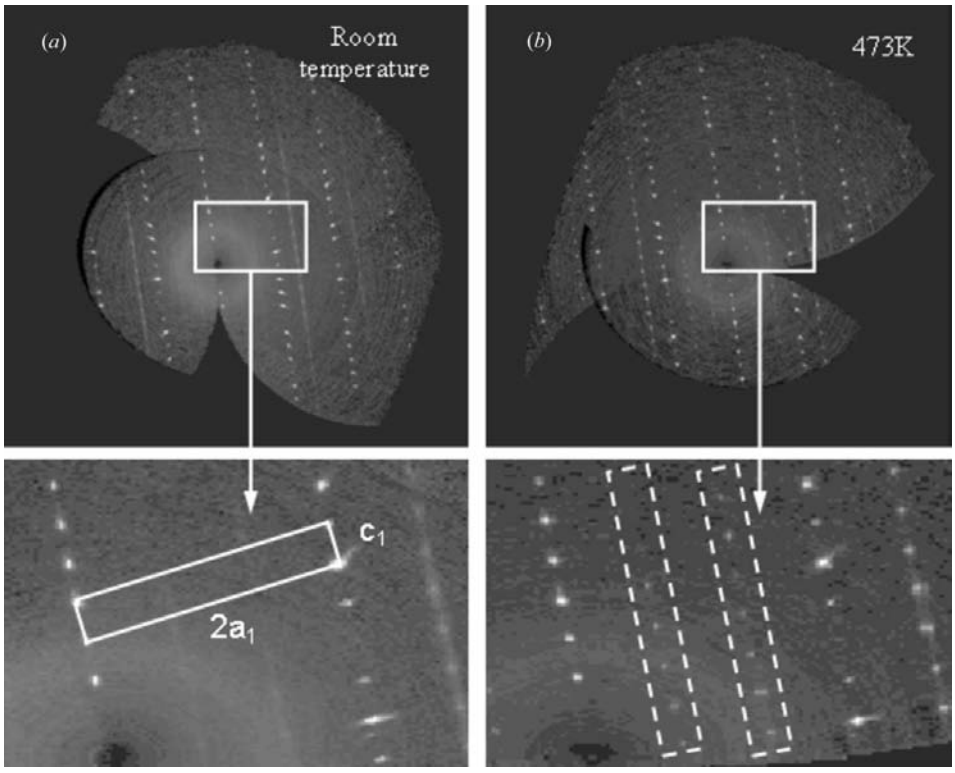

Figure 2
Reconstructed (*h*0*l*) reciprocal planes at (*a*) room temperature and (*b*) 473 K. Dashed line: $\mathbf{q}_2$ reflections and solid line: $2a_1$, c_1 cell.

performed between room temperature and 773 K: between 293 and 473 K every 10 K, then at 573 and 773 K.

A complete data collection was performed at 473 K using φ–ω scans with $0 < \theta < 45^\circ$ in steps of 0.3° per frame and a sample–detector distance of 34 mm. The two usual types of subsystems are easily recognized, and the lattice parameters are close to the room-temperature ones: a_1 = 4.839 (1), b_1 = 4.553 (1), b_2 = 2.8178 (5), c_1 = 10.858 (3) Å, β_1 = 98.12 (2)°. The misfit ratio is $\delta = b_1/b_2$ = 1.6157 (7). Data reduction and integration was performed using the *EVALCCD* software (Duisenberg *et al.*, 2003) in four independent datasets:

(i) main reflections compatible with the first cell (a_1, b_1, c_1, β_1),

(ii) main reflections compatible with the second one (a_2, b_2, c_2, β_2),

(iii) first-order satellite reflections for $\mathbf{q}_1 = (b_1/b_2)\mathbf{b}_2^* + \mathbf{a}_1^*$ and

(iv) first-order satellite reflections for $\mathbf{q}_2 = \frac{2}{3}\mathbf{a}_1^* - \frac{1}{3}\mathbf{c}_1^*$ vectors.

Lorentz and polarization corrections were made to the data. An analytical absorption correction using the morphology of the crystal based on the measurement of the crystal face orientation was performed with the *JANA*2000 software (Petříček & Dusek, 2000). The different datasets were then rescaled using common reflections, merged and averaged using the *JANA*2000 software. For the structure refinement, the data collection procedure and the general five-dimensional indexing of the reflections, the same approach as previously described was chosen, in order to keep the same basic cells. As it is not possible to deal simultaneously with an incommensurate scheme (q_1) and a commensurate one (q_2), a commensurate approximant was chosen, considering $\delta = b_1/b_2$ = 1.6157 (7) $\simeq$ 13/8. The structure refinement was developed in the five-dimensional formalism using the RS subcell as a reference basic cell (Muguerra *et al.*, 2008). Crystal data are summarized in Table 1.[1]

3. Structural phase transition and structure refinement

The present misfit CCO structure was previously studied as a commensurately modulated misfit structure (Muguerra *et al.*, 2008). This analysis was based on the observation at room temperature of extra weak satellite reflections described by the $\mathbf{q}_2 = \frac{2}{3}a_1^* - \frac{1}{3}c_1^*$ vector in the RS block diffraction pattern. They were interpreted with a partial ordering of the split atomic sites of the central [CoO] layer along **a** (Muguerra *et al.*, 2008), resulting in a triple chain configuration. Nevertheless, these reflections are very weak and are also characterized by diffuse scattering along $\mathbf{c}^*$. This feature is coherent with the refined residual atomic disorder along the misfit **b** direction corresponding to a split-atom model for the Co and O atomic sites of the central layer. Our present study as a function of the temperature shows that these weak and rather diffuse reflections, observed at 293 K, become more condensed at high temperature and others (too weak at room temperature to be seen) become visible. Their intensities rapidly increase around 400 K and finally reach a constant maximal value (Figs. 2 and 3*a*). This feature is reversible and reproducible. This intensity modification is not observed for the main reflections of the two sublattices (Fig. 3*b*). These observations are quite unexpected because such satellite reflections, which are most of the time associated with a modulated ordering of the structure, usually appear when cooling down the crystal. It can then be assumed that their intensity variations result from a modification of the structural configuration of the [CoO] layer; this point requires a new structure refinement at high temperature.

[1] Supplementary data for this paper are available from the IUCr electronic archives (Reference: SN5073). Services for accessing these data are described at the back of the journal.

The single-crystal X-ray diffraction study was performed at 473 K and the corresponding intensity dataset was used for the refinement. The crystal symmetry is compatible with previous studies. The superspace group is still $C2/m(1\delta0)(\alpha0\gamma)gm$ with $\alpha = \frac{2}{3}$ and $\gamma = -\frac{1}{3}$. However, at 473 K in ($h0l$), ($h1l$) and ($h2l$) planes (Fig. 2), the weak reflections characterizing the $\mathbf{q}_2 = \frac{2}{3}\mathbf{a}_1^* - \frac{1}{3}\mathbf{c}_1^*$ modulation are measured with a larger intensity than at room temperature.

The refinement was performed using the room-temperature atomic positions and modulations as starting points. One can first recall that the role of the commensurate triple $\mathbf{q}_2$ modulation of the room-temperature model was to discriminate three different physical sections involved in the structural description. As a matter of fact, only the sections corresponding to the phase variable $u = x_5 - \mathbf{q}_2\mathbf{r} = 0, \frac{1}{3}$ and $\frac{2}{3}$ (where $\mathbf{r}$ is the reference atomic position of the Co or O atoms) are now present in the commensurately modulated crystal. The apparent disordered splitting (Grebille *et al.*, 2004) of the Co1*a*, Co1*b*, O2*a* and O2*b* sites along x_1 disappears in a superstructure with triple Co—O chains (Muguerra *et al.*, 2008) along the **b** direction. Only a residual disorder along x_2 still exists concerning the Co1*b* and O2*b* atomic sites. At 473 K the agreement factors with this model are rather good, but the observed Fourier maps around the Co and O split sites of the [CoO] layer show significant changes (Fig. 4). Looking at the electron densities corresponding to the high-temperature refinement, one can see that the room-temperature disorder disappears. In Fig. 5 corresponding probability density functions are compared between 473 and 273 K. Curves with two distinct maxima at room temperature are replaced by new curves with only one maximum. This shows that the split-atom model is no longer relevant at high temperature and can be replaced by a single more symmetrical atomic site, both for Co and O. This requires a change of the structural model: the x_2 values for the Co1*b* and O2*b* atoms are now very close to 0 or $\frac{1}{2}$. New models were then tested to describe this new atomic configuration. The best results were obtained with an off-center O2*a* site and with two Co1*a* and Co1*b* sites with x_2 values constrained to $\frac{1}{2}$ and 0 (against 0.42 for O2*b* and 0.067 for Co1*b* at room temperature). For Co1*b* and O2*a*, anisotropic displacement parameters have been chosen, their refined values are large in the x_2 direction. The other atoms (Ca, O1, Co1*a*, Co2 and O3) keep the same room-temperature positions. Results for this new refinement are reported in Tables 2 and 3.

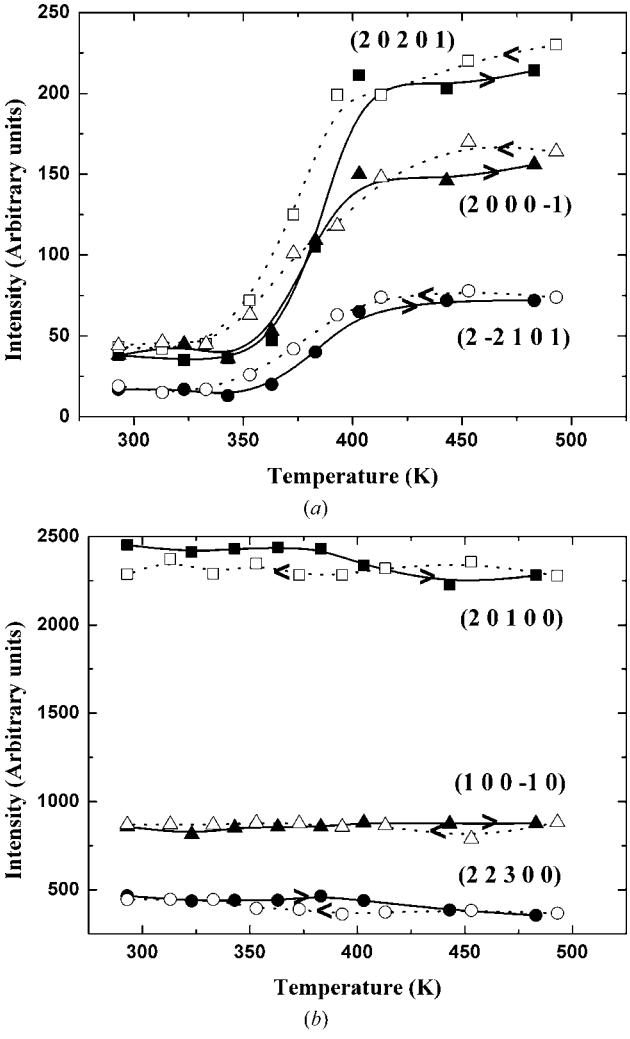

Figure 3
Intensity of some selected lines: (*a*) satellite reflections related to the commensurate modulation, (*b*) main reflections related to the first, the second, and to both sublattices of the misfit structure.

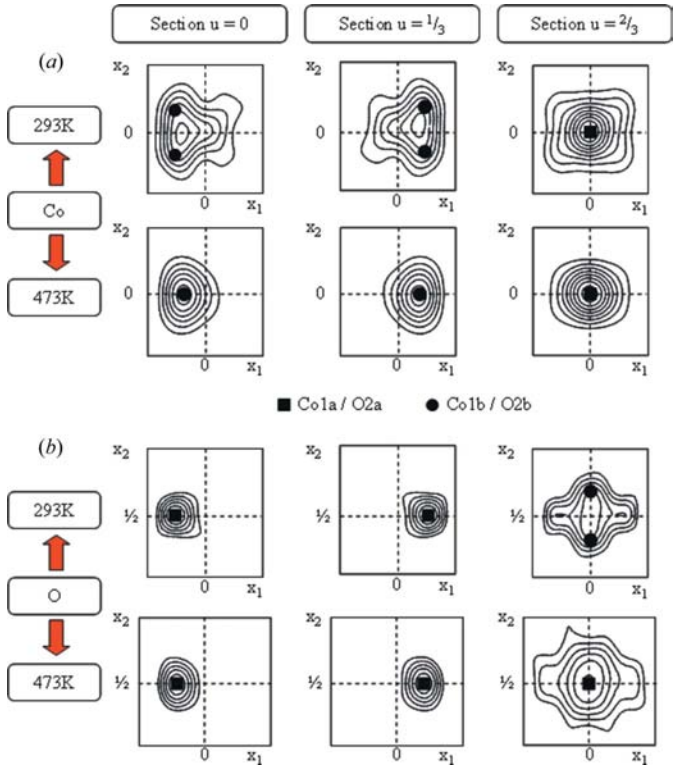

Figure 4
Observed Fourier maps of (*a*) Co and (*b*) O atoms within the [CoO] layer for three different sections at room temperature and 473 K.

Table 2
Atomic positions and modulation functions.

Atom	Wave	Occupancy	x_1	x_2	x_3	U_{iso}
First subsystem						
Ca		1	0.43024 (7)	0†	0.27564 (3)	0.01225 (12)
	sin ($2\pi x_4$)	–	−0.0150 (2)	0†	0.00029 (13)	–
	cos ($2\pi x_4$)	–	0†	−0.0026 (4)	0†	–
	sin ($2\pi x_5$)	–	0.00164 (19)	0†	0.00098 (10)	–
	cos ($2\pi x_5$)	–	0.00099 (19)	0†	0.00593 (10)	–
O1	–	1	0.0529 (2)	0†	0.66415 (10)	0.0142 (4)
	sin ($2\pi x_4$)	–	−0.0029 (8)	0†	−0.0010 (4)	–
	cos ($2\pi x_4$)	–	0†	−0.0028 (12)	0†	–
	sin ($2\pi x_5$)	–	−0.0037 (6)	0†	0.0016 (3)	–
	cos ($2\pi x_5$)	–	−0.0025 (5)	0†	−0.0061 (3)	–
Co1*a*		0.26 (3)	0†	0†	0.5	0.0103 (11)
	sin ($2\pi x_4$)	0†	−0.0025 (16)	0†	0‡	–
	cos ($2\pi x_4$)	0†	0†	0†	0†	–
	sin ($2\pi x_5$)	0†	−0.071 (6)	0†	0.004 (3)	–
	cos ($2\pi x_5$)	−0.25 (2)	0†	0‡	0†	–
Co1*b*	–	0.708 (15)	0.0686 (14)	0†	0.5001 (4)	0.0317 (6)
	sin ($2\pi x_4$)	0‡	−0.0063 (10)	0†	−0.0005 (2)	–
	cos ($2\pi x_4$)	0‡	0†	0†	0†	–
	sin ($2\pi x_5$)	0.194 (5)	0.007 (2)	0†	−0.0011 (4)	–
	cos ($2\pi x_5$)	0.009 (4)	0.0302 (17)	0†	0‡	–
O2*a*	–	0.968 (5)	0.0671 (17)	0.5	0.5003 (3)	0.0284 (17)
	sin ($2\pi x_4$)	0‡	0.009 (4)	0†	0‡	–
	cos ($2\pi x_4$)	0†	0†	0.009 (5)	0†	–
	sin ($2\pi x_5$)	0.369 (14)	0.038 (4)	0†	0‡	–
	cos ($2\pi x_5$)	−0.104 (9)	0.031 (5)	0†	−0.0032 (15)	–
Second subsystem						
Co2	–	0.950 (2)	0.75	0.75	0†	0.00545 (10)
	sin ($2\pi x_4$)	–	0†	0†	0†	–
	cos ($2\pi x_4$)	–	0.00553 (11)	0†	0.00414 (5)	–
	sin ($2\pi x_5$)	–	−0.00071 (19)	0†	0.00044 (10)	–
	cos ($2\pi x_5$)	–	0†	0†	0†	–
O3	–	0.976 (5)	0.3861 (2)	0.75	−0.09310 (9)	0.0089 (3)
	sin ($2\pi x_4$)	–	0†	0.0030 (9)	0†	–
	cos ($2\pi x_4$)	–	0.0069 (4)	0†	0.00298 (17)	–
	sin ($2\pi x_5$)	–	−0.0022 (6)	0†	0‡	–
	cos ($2\pi x_5$)	–	0.0012 (6)	0†	0‡	–

Table 3
Refined anisotropic displacement parameters.

Atom	U^{11}	U^{22}	U^{33}	U^{12}	U^{13}	U^{23}
Ca	0.0113 (2)	0.0135 (2)	0.0117 (2)	0†	0.00090 (15)	0†
O1	0.0167 (7)	0.0162 (7)	0.0097 (7)	0†	0.0017 (5)	0†
Co1*b*	0.0195 (12)	0.0723 (11)	0.0032 (6)	0†	0.0015 (6)	0†
O2*a*	0.005 (4)	0.068 (2)	0.0111 (13)	0†	0‡	0†
Co2	0.00421 (15)	0.0062 (2)	0.00588 (14)	0†	0.00061 (16)	0†
O3	0.0063 (5)	0.0098 (8)	0.0105 (5)	0†	0.0008 (4)	0†

† Fixed to zero by symmetry. ‡ Fixed to zero as non-significant.

4. Discussion

4.1. Structural evolution of the central [CoO] layer

As can be seen on the summed observed Fourier maps, the structural transition can be associated with a modification of the central [CoO] layer of the *RS* subsystem. Two types of map can be used: the summed Fourier maps as a function of x_1 and x_5, and as a function of x_1 and x_2 (Figs. 6*a* and 7*a*). They must be interpreted in relation to the variations of the Co and O site occupancies within the [CoO] layers (Figs. 6*b* and 7*b*).

In Fig. 4, the three physically significant x_1–x_2 sections of the supercrystal are shown in the vicinity of the Co (Fig. 4*a*) and the O (Fig. 4*b*) atoms, and compared between room temperature and 473 K. The main conclusion is that the electronic density is partially split at room temperature, and described by disordered atomic positions. It is centred at high temperature at $x_2 = 0$, for both the Co and O atoms, so that we could imagine only one modulated atomic site to explain the displacement along x_1 for these atoms. This feature is confirmed by the regular and continuous appearance of the electron density in the x_1–x_5 sections compared with the corresponding ones at room temperature (Muguerra *et al.*, 2008). Nevertheless, a more careful examination of these different densities and the refinement process have shown that the simulation is improved when considering two or three atomic sites in each case, but in a very different configuration than at room temperature. As will be explained in the following, these atomic sites are no longer needed to describe a split-atom disordered model, but to represent a continuous unique modulated atomic site reflecting more accurately the extended electron density of the x_1–x_5 maps.

For Co atoms at room temperature, these maps are characterized by three maxima corresponding to the three commensurate sections (Muguerra *et al.*, 2008). However, at 473 K this inhomogeneous density is replaced by a constant continuous distribution. The position modulations are more important than at room temperature (Fig. 4*a*): the Co1*a* position modulation describes the biggest part of the density. The modulation functions which represent Co1*a* and Co1*b* are continuous and complement each other. The Co site is now globally described by only one displacive modulation function close to a sawtooth modulation. Sawtooth-function parameters cannot be refined in the five-dimensional description with the software *JANA*2000 (Petříček & Dusek, 2000); moreover, keeping harmonic modulation functions allows us to compare the different structures with an equivalent structural model. For the O2*a* atoms, two regions of high density still exist on the Fourier maps observed as a function of x_1 and x_5 (Fig. 6*a*). They correspond to the sections $u = 0$ and $u = \frac{1}{3}$; the $u = \frac{2}{3}$ section is more problematic. Looking at the occupation modulation functions, the two first sections correspond to a maximized occupation for each individual O2*a* site coupled with the largest displacement of the atom from the $x_1 = 0$ position. The section $u = \frac{2}{3}$ corresponds to the merging of two half-occupied symmetry-related O2*a* sites near the $x_1 = 0$ value, so that it is practically equivalent to a unique fully occupied site, comparable with the two first displaced positions. Finally, the two eccentric symmetry-related modulated sites are also equivalent to one atomic cord describing a global modulated electronic density.

The [CoO] layer can be described by triple chains running along the *b* misfit direction, orthogonal to the $\mathbf{q}_2$ modulation (Fig. 8), resulting from in-phase negative, zero or positive x_1

modulated displacement of the Co and O atoms. The same type of chain was observed at room temperature (Muguerra *et al.*, 2008; Fig. 8*a*). However, in this last case the Co and O atoms were partially described by split sites along **b**, and this was responsible for a residual disorder in this direction. This splitting was interpreted by a local arrangement of clusters. At 473 K, the x_2 splitting disappeared and the probability density functions corresponding to the atomic sites only have one centred maximum. The corresponding disorder also disappeared and the general configuration of the chain was more regular (Fig. 8*b*). Some O sites still show a small splitting along **a** at 473 K, but these are very close together. They correspond to the previously described $u = \frac{2}{3}$ section of the O site. Here we can consider them to be one position which results from the summation of the two.

A perfect and regular *RS* stacking compatible with lattice parameters in this [CoO] layer should result in Co—O distances which are too large, equivalent to the Ca—O distances in the neighbouring regular Ca—O layers (between 2.36 and 2.51 Å). Along **b**, the corresponding Co—O distance 2.28 Å is obtained. (The Ca—O distance is a little larger because the Ca and O atoms are not coplanar.) Along **a**, the triple configuration leads to reasonable Co—O distances (1.88 Å for the central Co atom and 2.05 Å for the peripheral ones). The Co atoms are also bound to O atoms of the [CaO] layers: Co1*a*—O = 1.765 (1) and Co1*b*—O = 1.797 (4) or 1.793 (5) Å. The central Co atom corresponds to the non-displaced Co1*a* atom in an octahedral O environment; the peripheral ones are modelled by the Co1*b* sites and bound to only five O atoms. The corresponding calculated bond valences (Brese & Keeffe, 1991) are +2.3 for Co1*a* and +3.3 for Co1*b*, confirming the mixed +2/+3/+4 valence of Co atoms in this complex layer.

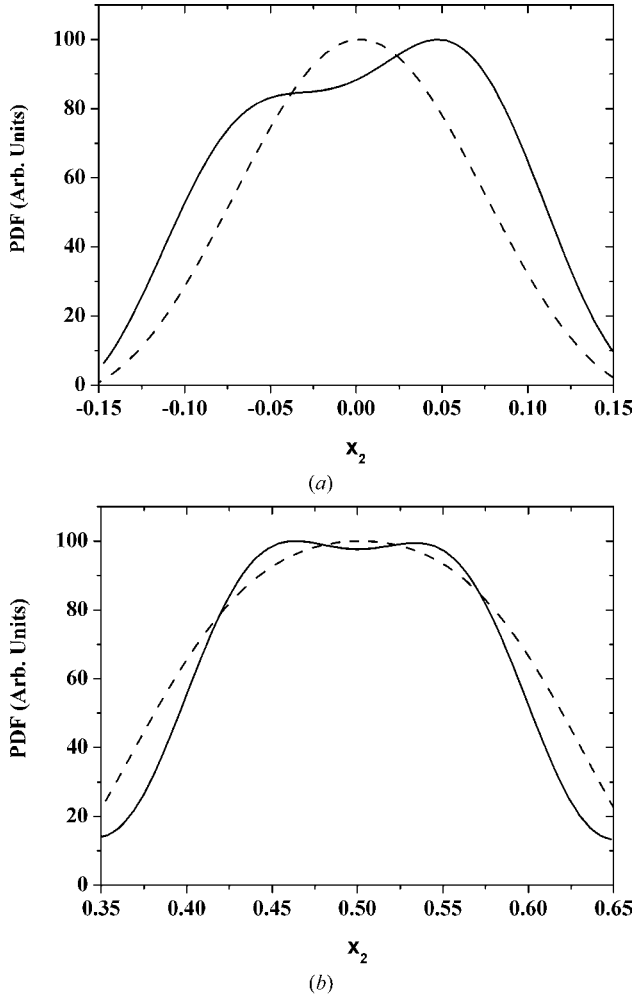

Figure 5
Probability density functions as a function of x_2 (*a*) for the Co atom at $x_1 \simeq 0.1$ and $u = 0$, and (*b*) for the O atom at $x_1 = 0$ and $u = \frac{2}{3}$. Solid line: room temperature; dashed line: 473 K.

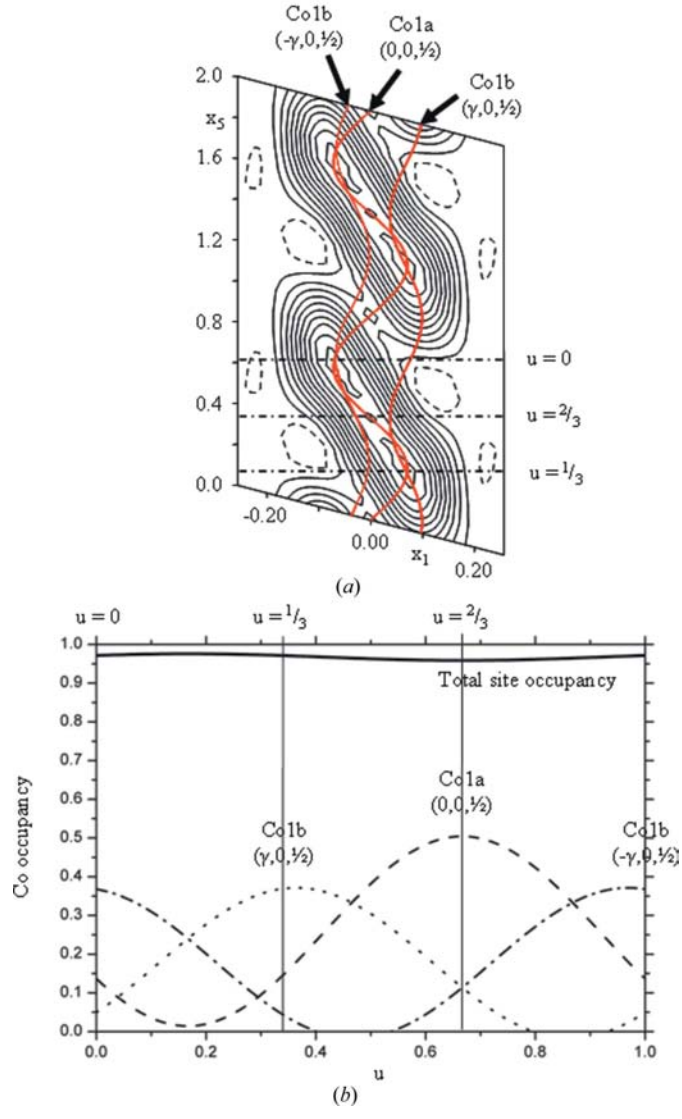

Figure 6
(*a*) Observed Fourier maps of the Co atoms and (*b*) variations of the Co occupancy within the [CoO] layer (u is given by $u = x_5 - \mathbf{q}_2\mathbf{r}$). The different Fourier maps as a function of x_1 and x_5 have been summed along the x_2 and x_3 coordinates.

4.2. Unchanged layers and connections between the different layers

The modifications within the [CoO] layers do not affect the [CaO] and the [CoO_2] layers. In the [CoO_2] layers, the compression of the CoO_6 octahedra along **c** is still observed. This distortion affects the basal planes of the octahedra (distances O—O = 2.80 and 2.58 Å) and O—Co—O angles (85 or 95°), but not the Co—O distances (∼ 1.90 Å). The calculated bond valence of Co atoms is +3.5 using Brese & O'Keeffe (1991) parameters, or +3.36 with reference to the Li_xCoO_2 system (Levasseur, 2001). The temperature did not affect the valence of the Co atoms of this layer. In the [CaO] layers, the Ca sublattice is slightly translated with respect to the O layer. The modifications of these two types of layers are linked, indeed they can be explained as an adjustment between the O atoms of the [CoO_2] layers and the Ca atoms of [CaO] layers in order to promote Ca—O interactions between the two subsystems [Ca—O distances: 2.327 (8) or 2.283 (8) Å]. The Ca—O distances are close to 2.3 Å which corresponds to a strong bond between both subsystems.

Some interactions exist between the [CoO] continuous chains and the [CaO] layers: Co—O and Ca—O inter-layer interactions. The Co—O distances lie between 1.765 (1) and 1.797 (4) Å and Ca—O between 2.431 (9) and 2.436 (9) Å. The changes observed within the [CoO] layers do not significantly affect the two other types of layers or the interaction between these layers.

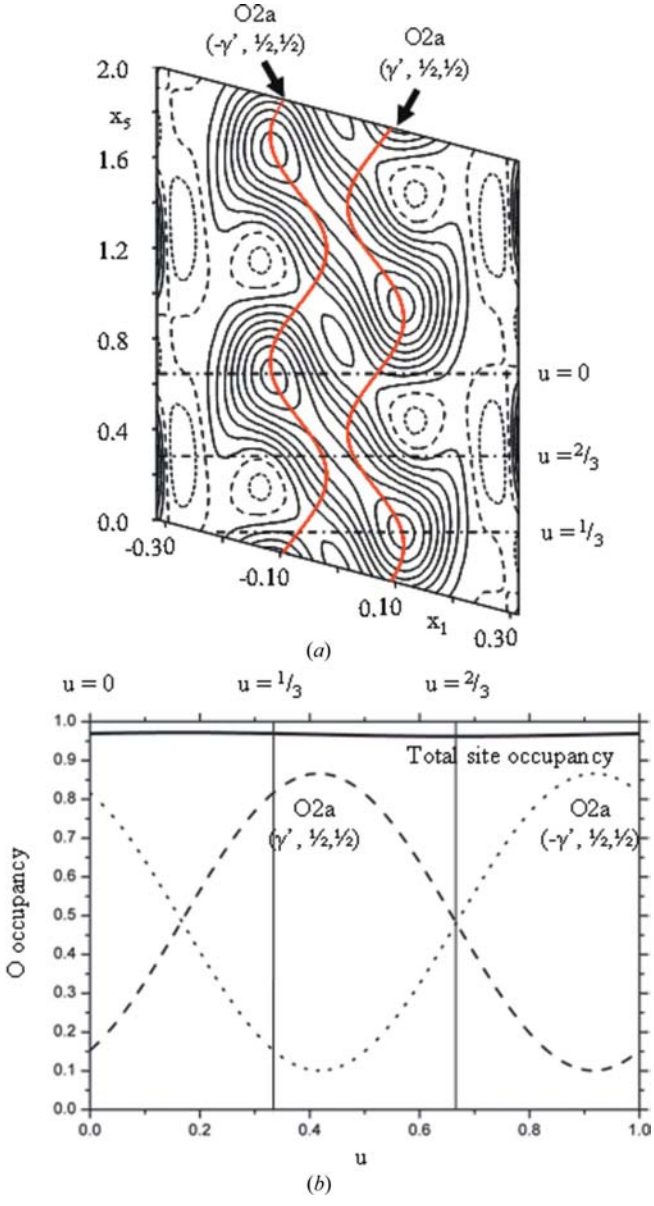

Figure 7
(*a*) Observed Fourier maps of the O atoms and (*b*) variations of the O occupancy within the [CoO] layer (u is given by $u = x_5 - \mathbf{q}_2\mathbf{r}$). The different Fourier maps as a function of x_1 and x_5 have been summed along the x_2 and x_3 coordinates.

5. Conclusion

A structural phase transition has been characterized around 400 K involving a change in the modulated $\mathbf{q}_2$ scheme of the central [CoO] layer of the misfit lamellar structure $[Ca_2CoO_3][CoO_2]_{1.62}$. A disordered arrangement was recently described concerning this layer, with a partial split-atom model allowing a triple chain configuration along the **b** direction (Muguerra *et al.*, 2008). At higher temperatures, the atomic split double sites are replaced by unique sites, so that this transition can be interpreted as a disorder–order transition. In the present case, the high-temperature phase is the ordered one, with a more regular configuration compared with the likely disordered clustering proposed for the room-temperature phase. A higher degree of coherence is then obtained between the layers of this lamellar structure, consistent with the condensation of rather diffuse diffraction satellite nodes into more intense and condensed satellite reflections. The origin of this transition can be attributed to the cell parameter mismatch between the different layers of the lamellar structure. As a matter of fact, the [CoO_2] slab and the [CaO] layer adapt themselves to each other through the misfit structure and the related modulated displacements lead to relatively constant inter-subsystem Ca—O distances close

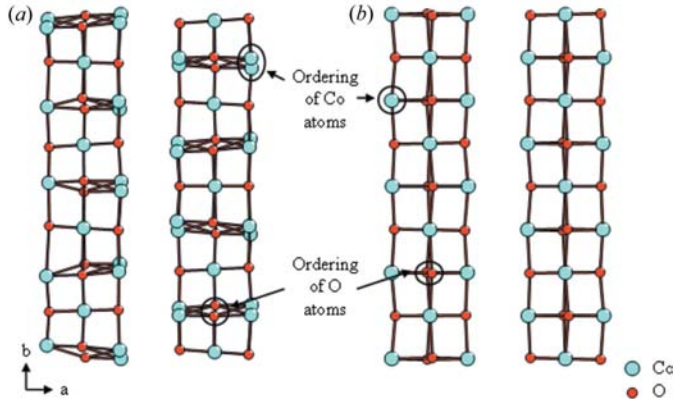

Figure 8
Schematic representation of the [CoO] layer projected along **c** (*a*) at room temperature and (*b*) at 473 K.

to 2.3 Å. However, at room temperature the oxygen environment of Co is not compatible with the planar cell parameters of the [CaO] layer. Accommodation is first made by a triple-chain configuration resulting in octahedral and pyramidal Co environments, and second by an average disorder along **b** probably resulting from a local arrangement in clusters. Increasing the temperature probably enables a local and weak dilatation of the Co—O bonds in this direction, so that the disorder is reduced and the configuration becomes quite regular, with a recovering of a perfect translational order. A similar and more spectacular ordering has also been recently described with the three-layered sodium cobaltite P'_3-$Na_{0.62}CoO_2$ (Blangero *et al.*, 2008). The Na rearrangement around 350 K corresponds to the occupation of more symmetrical sites and consequently to a global symmetry change.

Recent comparisons between Na_xCoO_2 and CCO have shown that physical properties associated with the electronic configuration of the $[CoO_2]$ layers cannot be explained only in the framework of this lone layer, but electronic and coulombic interactions with the doping *RS* block have to be considered. The present phase transition confirms this dependence, because the observed weak structural modification only concerns the central layer of the *RS* block; it results in a more regular ordering of the Co and O sites, and leaves the rest of the structure, in particular the $[CoO_2]$ layer, unchanged. Nevertheless, it can be associated with physical phase transitions which were shown through electric and magnetic physical measurements (Masset *et al.*, 2000). A slight increase of the electrical conductivity of the compound (which is localized in the $[CoO_2]$ layers) is observed at the same temperature range. A slight change in the magnetic susceptibility of this phase is also simultaneously observed, which can be the consequence of new magnetic interactions in relation to the variations of interatomic distances. However, the origin of this feature is still to be clarified in relation to the double mixed valence of Co in both subsystems.

The authors thank Hélène Rousselière for technical assistance and X-ray diffraction data collection and Olivier Pérez for helpful discussions.

References

Argoud, R. & Capponi, J. J. (1984). *J. Appl. Cryst.* **17**, 420–425.
Blangero, M., Carlier, D., Pollet, M., Darriet, J., Delmas, C. & Doumerc, J. P. (2008). *Phys. Rev. B*, **77**, 184116 (1–8).
Bobroff, J., Hébert, S., Lang, G., Mendels, P., Pelloquin, D. & Maignan, A. (2007). *Phys. Rev. B*, **76**, 100407 (1–4).
Brese, N. E. & O'Keeffe, M. (1991). *Acta Cryst.* B**47**, 192–197.
Duisenberg, A. J. M., Kroon-Batenburg, L. M. J. & Schreurs, A. M. M. (2003). *J. Appl. Cryst.* **36**, 220–229.
Funahashi, R., Matsubara, I., Ikuta, H., Takeuchi, T., Mizutaniand, U. & Sodeoka, S. (2000). *Jpn. J. Appl. Phys.* **39**, L1127–L1129.
Grebille, D., Lambert, S., Bourée, F. & Petříček, V. (2004). *J. Appl. Cryst.* **37**, 823–831.
Grebille, D., Muguerra, H., Pérez, O., Guilmeau, E., Rousselière, H. & Funahashi, R. (2007). *Acta Cryst.* B**63**, 373–383.
Koshibae, W., Tsutsui, K. & Maekawa, S. (2000). *Phys. Rev. B*, **62**, 6869–6872.
Lambert, S., Leligny, H. & Grebille, D. (2001). *J. Solid State Chem.* **160**, 322–331.
Levasseur, S. (2001). Thesis, ICMCB University of Bordeaux 1, France.
Li, S., Funahashi, R., Matsubara, I., Ueno, K. & Yamada, H. (1999). *J. Mater. Chem.* **9**, 1659–1660.
Limelette, P., Hardy, V., Auban-Senzier, P., Jérôme, D., Flahaut, D., Hébert, S., Frésard, R., Simon, C., Noudem, J. & Maignan, A. (2005). *Phys. Rev. B*, **71**, 233108 (1–4).
Limelette, P., Hébert, S., Hardy, V., Frésard, R., Simon, C. & Maignan, A. (2006). *Phys. Rev. Lett.* **97**, 046601 (1–4).
Ling, C. D., Aivazian, K., Schmid, S. & Jensen, P. (2007). *J. Solid State Chem.* **180**, 1446–1455.
Masset, C., Michel, C., Maignan, A., Hervieu, M., Toulemonde, O., Studer, F. & Raveau, B. (2000). *Phys. Rev. B*, **62**, 166–175.
Miyazaki, Y., Kudo, K., Akoshima, M., Ono, Y., Koike, Y. & Kajiitani, T. (2000). *Jpn. J. Appl. Phys.* **39**, L531–L533.
Miyazaki, Y., Onoda, M., Oku, T., Kikuchi, M., Ishii, Y., Ono, Y., Morii, Y. & Kajitani, T. (2002). *J. Phys. Soc. Jpn.* **71**, 491–497.
Muguerra, H., Grebille, D. & Bourée, F. (2008). *Acta Cryst.* B**64**, 144–153.
Petříček, V. & Dusek, M. (2000). *JANA*2000. Institute of Physics, Praha, Czech Republic.
Sugiyama, J., Brewer, J. H., Ansaldo, E. J., Itahara, H., Dohmae, K., Seno, Y., Xia, C. & Tani, T. (2003). *Phys. Rev. B*, **68**, 134423 (1–8).
Sugiyama, J., Xia, C. & Tani, T. (2003). *Phys. Rev. B*, **67**, 104410 (1–5).
Terasaki, I., Sasago, Y. & Uchinokura, K. (1997). *Phys. Rev. B*, **58**, R12685–R112687.
Xia, C., Sugiyama, J., Itahara, H. & Tani, T. (2005). *J. Cryst. Growth*, **276**, 519–524.
Xiang, H. J. & Singh, D. J. (2007). *Phys. Rev. B*, **76**, 195111 (1–5).
Yamamoto, A. (1992). *Acta Cryst.* A**48**, 476–483.